

Numerical Heat Transfer, Part B: Fundamentals

An International Journal of Computation and Methodology

ISSN: 1040-7790 (Print) 1521-0626 (Online) Journal homepage: <https://www.tandfonline.com/loi/unhb20>

Numerical modeling of interfacial heat and mass transport phenomena during a phase change using ANSYS-Fluent

Isaac Perez-Raya & Satish G. Kandlikar

To cite this article: Isaac Perez-Raya & Satish G. Kandlikar (2016) Numerical modeling of interfacial heat and mass transport phenomena during a phase change using ANSYS-Fluent, Numerical Heat Transfer, Part B: Fundamentals, 70:4, 322-339, DOI: [10.1080/10407790.2016.1215708](https://doi.org/10.1080/10407790.2016.1215708)

To link to this article: <https://doi.org/10.1080/10407790.2016.1215708>



Published online: 06 Oct 2016.



Submit your article to this journal [↗](#)



Article views: 654



View related articles [↗](#)



View Crossmark data [↗](#)



Citing articles: 3 View citing articles [↗](#)

Numerical modeling of interfacial heat and mass transport phenomena during a phase change using ANSYS-Fluent

Isaac Perez-Raya^a and Satish G. Kandlikar^{a,b}

^aDepartment of Microsystems Engineering, Rochester Institute of Technology, Rochester, NY, USA; ^bDepartment of Mechanical Engineering, Rochester Institute of Technology, Rochester, NY, USA

ABSTRACT

Numerical modeling of phase change requires accurate estimations of heat and mass transport at the interface. The present work develops a model in ANSYS-Fluent with user-defined functions to address phase change with a planar interface. An interface boundary method determines the heat fluxes with the exact location of the interface without interpolation functions. Five cases are analyzed based on the classic Stefan problem for validating the model. The numerical model is validated against closed form theoretical solutions with agreement within 0.55%. This work can be extended to include curvature effects and the interaction between the interface and heterogeneous surfaces.

ARTICLE HISTORY



Received 23 May 2016

Accepted 23 June 2016

1. Introduction

Phase change is widely used for cooling and energy storage applications since it utilizes latent heat as against sensible heat transfer. However, the underlying physics are complex as they involve heat transfer within the phases, interface motion due to mass transfer, and expansion due to density difference, just to mention a few. The analysis of phase change has been addressed by numerical modeling, which gives detailed temperature and velocity distributions in both phases and evolution of mass transfer across the interface. Also, numerical modeling provides control of the operating conditions, which allows the creation of multiple scenarios such as high wall superheats or density differences. However, to validate the accuracy of the simulation, a robust verification procedure using theoretical models is required. This work performs the validation of a numerical model for phase change with energy transfer within two phases and with density difference.

Stefan formulated the relation between temperature distribution and mass transfer across the interface between two phases [1]. In this model, heat flows in only one Cartesian direction and therefore the interface remains flat. The mass transfer depends on temperature gradients at the interface, and the interface remains at saturation temperature. Under these conditions, the enthalpy and mass conservation equations are solved to obtain theoretical solutions for the interface displacement and temperature distributions in both phases. Various versions of Stefan problems include heat transfer in only one phase, heat transfer in both phases, and the effect of density difference between the two phases [2]. In one-phase Stefan problems, heat travels through only one phase, and the mass transfer occurs without heat conduction in the other phase, since it is at the saturation state. In two-phase Stefan problems, heat travels through both phases, and the mass transfer depends on the temperature gradients on both sides of the interface. Stefan problems with density effect account for the expansion

CONTACT Satish G. Kandlikar  sgkeme@rit.edu  Department of Mechanical Engineering, Rochester Institute of Technology, 76 Lomb Memorial Drive, Rochester 14623-5604, NY, USA.

Color versions of one or more of the figures in this article can be found online on at www.tandfonline.com/unhb.

© 2016 Taylor & Francis

Nomenclature

A_{int}	interface area in the cell (m^2)	t	time (s)
c_p	specific heat (J/kg K)	u	velocity (m/s)
dT	superheat/subcooled level (K)	V_{cell}	cell volume (m^3)
dy	cell length (m)	Y	analytic interface displacement (m)
F_1	phase 1 volume of fraction	y	y -coordinate (m)
\dot{h}	source term in the enthalpy equation (W/m^3)	α	thermal diffusivity (m^2/s)
k	thermal conductivity (W/m-K)	λ	growth rate constant
L	latent heat of evaporation (J/kg)	μ	dynamic viscosity (Pa s)
l	domain length (m)	ν	ratio of thermal diffusivities between phases
p	pressure (N/m^2)	ρ	density (kg/m^3)
T	temperature (K)	$\dot{\rho}$	mass source term (kg/s m^3)
		ϕ	ratio of densities between phases

that occurs in one of the phases during phase change due to density difference between the two phases.

Researchers have used Stefan problems to prove reliability of their heat and mass transfer algorithms in phase change simulation. However, it is common to adopt one-phase Stefan problems that either neglect or include density effects. Hardt and Wondra [3] simulated droplet evaporation and 2D film boiling. The simulation used Fluent with User-Defined Functions (UDFs) and Volume-of-Fluid (VOF) to track the interface. The model for mass transfer used the kinetic gas theory to calculate the evaporative mass flux. Comparisons against one-phase Stefan problem without density effect proved the accuracy of the numerical model for different liquid heat capacities and thermal conductivities. Minimal differences were justified with a thermal imbalance caused by a large difference between the heat capacities of liquid and vapor. Thakur et al. [4] used the meshless local Petrov–Galerkin method to solve solidification problems. This method creates arbitrary shapes (with trial functions) inside the domain to integrate the governing equations, which removes the need for an arbitrary mesh. The mass transfer model used temperature gradients at the interface, and the enthalpy method tracked the interface movement. The numerical results were compared against one-phase Stefan problems with a subcooled solid phase. Good agreement was found in terms of interface displacement and temperature distributions. Other test cases of 2D-solidification with regular and irregular geometries also showed good agreement between theoretical and numerical data. Sato and Niceno [5] simulated pool boiling with VOF, the mass transfer model used the heat fluxes at the interface. The results indicated that during nucleate boiling, the heat flux increases/decreases with the bubble expansion/necking with a minimum heat flux at bubble departure. The simulation proved its accuracy by showing good agreement with one-phase Stefan problems which neglect or consider density effects. Also, the numerical results were compared against bubble growth at zero and nonzero gravity with good agreement. There are several other phase change simulations that use one-phase Stefan problems to verify its accuracy [6–10]. Therefore, in simulations of phase change, it is common to prove the accuracy of phase change models by simulating cases in which heat transfer occurs only in one phase.

There are, however, situations in which the mass transfer and the overall thermal performance is strongly influenced by the heat transfer in both phases. This is because heat travels as sensible heat in both phases, which influences the amount of energy available for phase change. Also, the temperature gradients in both phases contribute to the mass transfer. To illustrate, Banerjee and Dhir [11] simulated heat transfer in both phases during film boiling. The results revealed that the liquid subcooling reduced the bubble growth rate due to the heat transfer from the interface to the liquid; moreover, thin thermal layers next to the interface in the liquid side (formed due to the rapid interface displacement) increased the surface heat dissipation. Gylys et al. [12] performed experiments on boiling crisis, which occurs when nucleate boiling regime transforms to film boiling regime. Hot solid spheres, blanketed by a vapor layer, were submerged into a subcooled pool of water. The result indicated that higher liquid subcooling levels resulted in shorter cooling times due to

an enhanced heat transfer rate. Moreover, the subcooling level affected the duration of the film boiling regime and the fluctuations of the heat transfer coefficient. Augspurger and Udaykumar [13] simulated phase change materials (PCMs) with aluminum fins that increased the heat transfer into the PCM. In the solid phase, heat was transferred by conduction, and in the liquid phase, convective currents increased the heat transfer which led to faster melting rates. Muhammad et al. [14] performed experiments and simulations on the melting of a PCM with heat transfer in liquid and solid phases. A hot wall melted the solid phase by transferring heat through the liquid phase. The results showed temperature differences along the radial direction in the solid phase, which provides evidence of heat transfer through the solid phase. In another application, cryosurgery is one of the most common techniques to treat cancer tumors. In this medical treatment, the heat transfer in both phases should be correlated to accurately estimate the freezing front which depends on the thermal properties of healthy and unhealthy tissues [15, 16]. These works prove the importance of analyzing phase change with heat transfer in both phases.

The purpose of this work is to describe a numerical model for phase change that simulates the heat transfer on both sides of the interface. One important requirement is the precise inclusion of the interface location as part of the numerical solution. This is performed by continuously tuning the temperature gradients of the cells next to the interface cell (neighboring cells) with the interface location. In essence, the interface position is used as a limit in the gradients of the neighboring cells. The simulation is performed in ANSYS-Fluent with UDFs that account for heat and mass transfer between the phases. The accuracy of the simulation is confirmed by comparing against theoretical solutions of one-phase and two-phase Stefan problems that neglect or consider density effects.

2. Model development

2.1. Computational domain

Figure 1 shows a schematic of the computational domain. It consists of a bottom plate and two phases, phases 1 and 2, separated by an interface. In one-phase Stefan problems, heat is transferred in one phase. In two-phase Stefan problems, heat is transferred in both phases. The domain is constrained by two vertical symmetry boundary conditions, a constant temperature at the bottom, and a constant temperature at infinite distance. This last condition is accomplished by setting this boundary far from the interface such that it does not influence the solution. The interface remains at saturation temperature and moves upwards due to the mass transfer from phase 2 to phase 1. Initially the interface is located at a certain position and the corresponding temperature distributions are determined from the theoretical solutions. In most of the simulations, the interface is initially located at $Y = 2dy$ where dy is the grid cell length. However, there are cases in which a thin thermal layer is present in

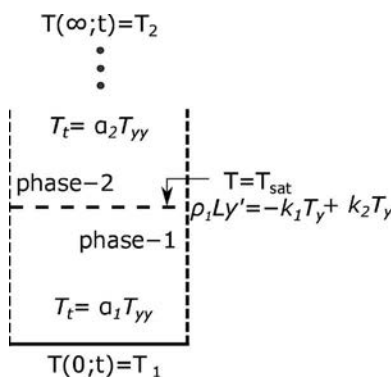


Figure 1. Schematic of two-phase Stefan problem.

phase 2. For these cases, the interface is initially located at length $Y(t = 0.1s)$, where Y is the theoretical interface displacement.

2.2. Governing equations

This section describes the governing equations for mass, momentum, energy, and interface tracking. Both fluids are considered incompressible and Newtonian. The mass conservation equation has the following form:

$$\nabla \cdot (\rho \mathbf{u}) = \dot{\rho} \quad (1)$$

In Eq. (1), $\dot{\rho}$ accounts for the mass transfer between phases, ρ is the density, and \mathbf{u} is the velocity field. The momentum conservation equation is given by Eq. (2).

$$\rho \left(\frac{\partial \mathbf{u}}{\partial t} + (\mathbf{u} \cdot \nabla) \mathbf{u} \right) = -\nabla p + \nabla \cdot \mu \nabla \mathbf{u} \quad (2)$$

where p represents the pressure field and μ is the viscosity. The enthalpy equation is given by Eq. (3).

$$\frac{\partial (\rho c_p T)}{\partial t} + \nabla \cdot (\rho c_p \mathbf{u} T) = \nabla \cdot (k \nabla T) + \dot{h} \quad (3)$$

where T is the temperature and \dot{h} is a source term that accounts for the heat that is removed during the phase change process, c_p is the specific heat, and k is the thermal conductivity. The VOF method tracks the interface displacement [17]. The VOF equation has the form of Eq. (4).

$$\frac{\partial F_1}{\partial t} + \mathbf{u} \cdot \nabla F_1 = \frac{\dot{\rho}}{\rho_1} \quad (4)$$

In Eq. (4), F_1 denotes the volume fraction of phase 1. The simulation assumes a sharp interface between phases 1 and 2. Therefore, F_1 assumes values of 1 or 0 in the phases and a value between 0 and 1 in the interface cell. Correspondingly, the phase 2 volume fraction is given as $1 - F_1$. The simulation uses Eq. (5) to assign the properties in each phase.

$$\zeta = F_1 \zeta_1 + (1 - F_1) \zeta_2 \quad (5)$$

where ζ is the corresponding property. Equation (5) also shows that the cells with an interface (interface cells) have properties which are average combinations of phases 1 and 2 properties. The average properties lead to errors in the simulation which may be minimized by decreasing the cell size. The mass transfer between phases is calculated with Eq. (6).

$$\dot{\rho} = \left(-\frac{k_1 \nabla T^-}{L} + \frac{k_2 \nabla T^+}{L} \right) \frac{A_{\text{int}}}{V_{\text{cell}}} \quad (6)$$

In Eq. (6), ∇T is the temperature gradient at the interface and L is the latent heat of evaporation, A_{int} is the interface area, and V_{cell} is the cell volume. The negative and positive signs in ∇T indicate phases 1 and 2 sides, respectively.

2.3. Numerical methods at the interface

Only a few works in the technical literature describe the numerical procedures around an interface. Fedkiw et al. [18] proposed the ghost fluid method which finds ghost temperatures and velocities in the interface cell by interpolating the temperatures within the active phase. Then, Gibou et al. [19]

applied this method to simulate one-phase Stefan problems with density effect using the level set method to track the interface. The numerical model was extended to simulate film boiling. The same method was adopted by Tanguy et al. [20] to simulate spherical bubble growth. The enthalpy equation was solved separately with ghost cells in which temperatures were linearly or quadratically determined. Relative to the linear extrapolation, a quadratic extrapolation improved the accuracy. The accuracy of the simulation decreased with the Jakob number due to a decrease in the thickness of the thermal boundary layer in the liquid side. Sato and Niceno [5] developed a VOF based phase change model that determined the mass transfer with the heat fluxes at the interface. The interface was smeared in three to five cells and it was identified with a volume-fraction of 0.5. A conservation equation maintained a sharp interface. The interface was located by changing the fluxes in the cells next to the interface with the interface position. The model used an extrapolation function to calculate the temperature gradients in the vapor side, and a second order central Taylor series formulation to determine the temperature gradients at the interface and in the neighboring cells on the liquid side. PCMs are commonly simulated with the enthalpy method, which defines a phase change temperature range to create a mushy interface region [4, 13, 14, 21]. The method uses the enthalpy to define the interface cells, and it is usually used without special numerical treatment of the interface cells.

The present work uses the standard discretization schemes in ANSYS-Fluent to estimate the fluxes in the neighboring cells with the interface location. The method identifies the interface with the F_1 value at the interface cell and uses the interface position as a boundary in the integrals of the neighboring cells. This interface boundary method precisely identifies the interface position in the solution of the enthalpy equation. The method works for nonsmeared interfaces. Also, it is free of extrapolation or interpolation functions. Therefore, the method is purely numerical which makes it easier to be implemented. To illustrate, consider the situation depicted in Figure 2. Assume that the interface cell (cell B) has a phase 1 volume of fraction of $0 < F_B < 1$. The integration of the diffusive term in the enthalpy equation over the control volume A (neighboring cell in the phase 1 side) from the cell face w to the interface position i gives Eq. (7).

$$\left(k_1 \frac{\partial T}{\partial x}\right)_i - \left(k_1 \frac{\partial T}{\partial x}\right)_w = k_1 \frac{(T_{\text{sat}} - T_A)}{\Delta x(0.5 + F_B)} - k_1 \frac{(T_A - T_w)}{\Delta x} \quad (7)$$

where T_A is the temperature of the neighboring cell in the phase 1 side, and T_w is the temperature next to the neighboring cell in the west side. Δx is the cell length, and F_B is the VOF value of the phase 1 in the cell B (interface cell). The flux at the interface is calculated with a backward difference approximation which is first-order accurate. The flux at the cell face 'w' is evaluated using a central difference approximation which is second-order accurate. The extended length of the neighboring cell A appears in the transient term and may be given by $\Delta x(1 + F_B)$. Similarly, Eq. (8) gives the fluxes on cell C (neighboring cell in the phase 2 side).

$$\left(k_2 \frac{\partial T}{\partial x}\right)_e - \left(k_2 \frac{\partial T}{\partial x}\right)_i = k_2 \frac{(T_C - T_E)}{\Delta x} - k_2 \frac{(T_{\text{sat}} - T_C)}{\Delta x(1.5 - F_B)} \quad (8)$$

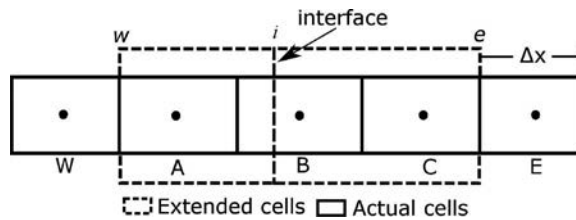


Figure 2. Interface boundary method for the exact location of the interface.

where T_C is the temperature of the neighboring cell on the phase 2 side, and T_E is the temperature next to the neighboring cell on the east side. In the integration at cell C, the flux at the interface is calculated with a forward difference approximation. The flux at the cell face 'e' is evaluated using a central difference approximation. The length of the extended cell C may be given by $\Delta x(2 - F_B)$. Equations (7) and (8) show that the interface boundary method determines the fluxes in the neighboring cells with the VOF value in the interface cell and with the interface temperature. The method lacks extrapolation functions to determine the interface cell temperature. In fact, the fluxes in the neighboring cells are independent of the temperature values in the interface cell (T_B), which means that the neighboring cells ignore the cell B. The neighboring cells are continuously extended with the VOF value to reach the interface position. The main advantage of ignoring cell B in computing the temperature gradients is that errors related to the use of average properties in the interface cells are eliminated. It is important to emphasize that the interface cell (cell B) is part of the solution of the enthalpy equation, but the information given by this cell is ignored by the neighboring cells. Therefore, the grid remains unchanged and only the estimation of the fluxes in the neighboring cells is adjusted. At other cells, the fluxes were evaluated using central difference approximation. The convective term was discretized in a manner similar to the diffusive term and further modified to account for the interface position. To satisfy the continuity equation, a divergence-free condition should be accomplished in the convective terms in each cell. This implies that the phase 2 velocity is used to estimate the convective terms at the cell-faces as discussed by Galione et al. [22]. For 2D and 3D simulations, similar equations can be derived. In these simulations, the F_B value may be replaced by the corresponding distance from the interface cell face (in the phase 1 side) to the interface (as described by Sato and Niceno [5]). This is an area that we are currently developing.

2.4. Mass transfer model

The same principles outlined in the previous section could be used to derive an expression to estimate the mass transfer that takes into account the exact location of the interface, Eq. (9). This expression estimates the temperature gradients at the interface in terms of the VOF value at the interface cell; this ensures an accurate mass transfer estimation.

$$\dot{p} = \frac{1}{L} \left[-k_1 \frac{(T_{\text{sat}} - T_A)}{\Delta x(0.5 + F_B)} + k_2 \frac{(T_C - T_{\text{sat}})}{\Delta x(1.5 - F_B)} \right] \frac{A_{\text{int}}}{V_{\text{cell}}} \quad (9)$$

It is important to observe that the temperature gradients at the interface in both phases are determined without interpolation functions. Also, the mass transfer model does not use any dimensionless constants to match the numerical results with the theoretical data. Previous simulations that have used ANSYS-Fluent and that determine the mass transfer using temperature gradients at the interface use such constants to adjust the mass transfer. For instance, Akthar and Kleis [23] used ANSYS-Fluent to develop a phase change model with adaptive grid refinement, the mass transfer model had a dimensionless constant of 2.75 which was needed to generate accurate interface displacements. Sun et al. [8] simulated film boiling in ANSYS-Fluent, the mass transfer model had a dimensionless constant of 2 that multiplied the thermal conductivity. The present work shows that dimensionless constants in the mass transfer model may not be required if the estimation of the fluxes in the neighboring cells is performed as described.

2.5. Software procedures

ANSYS-Fluent is a software that solves the governing equations of mass, momentum, and energy conservation. However, the software needs to be customized with UDFs to account for heat and mass transformation during the phase change process. Figure 3 shows a flowchart of the numerical procedures and software customization. First, the variables are initialized with UDF *INIT* that defines

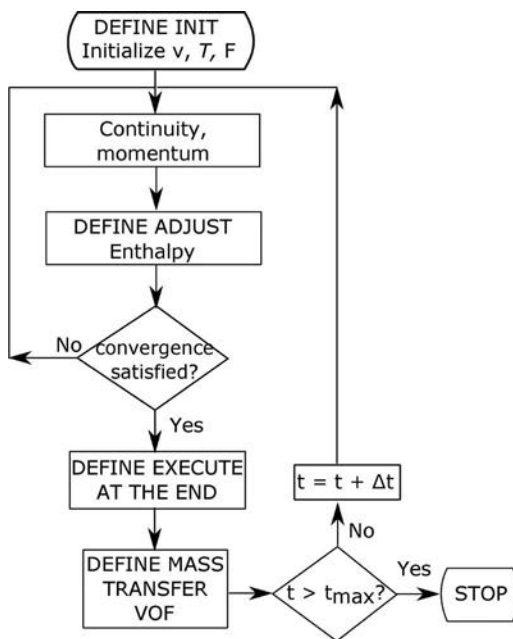


Figure 3. Flowchart of software procedures and customization.

values for VOF, temperature, and velocity. Second, the numerical model solves the continuity, momentum, and enthalpy equation. The SIMPLE algorithm solves the continuity and momentum equations. The enthalpy equation is adjusted with UDF *ADJUST* at every iteration with Eqs. (7) and (8). Third, the mass source terms are calculated, and the interface is advanced by the VOF equation, Eq. (4). The mass source terms are estimated with Eq. (9) at the end of each time step with UDF *EXECUTE AT END*. Then, the mass source terms are included in the VOF equation with UDF *MASS TRANSFER*. The simulation is completed when the ending time is reached or the cycle repeats with an extra time step. All the governing equations have a convergence criteria of 10^{-8} .

2.6. Study cases

The study cases are selected based on the heat transfer characteristics in film and pool boiling. In film boiling, a superheated vapor blanket covers the heated plate and a subcooled liquid lies next to the vapor blanket. In pool boiling, both phases are in contact with a heated plate, and therefore, both fluids may be superheated. For the validation of film boiling simulations, previous works have used one-phase Stefan problem with a growing superheated phase 1 and a consumed saturated phase 2 [3 7–9]. For the validation of pool boiling simulations, previous works have used sucking problem (one-phase Stefan problem with density effects), which has a consumed superheated phase 2, and a growing saturated phase 1 [5, 6, 24]. In both cases, one of the phases is always saturated. The present work considers five more cases whose main purpose is to provide more realistic examples for validation. These five cases are shown in Figure 4. In this figure, cases (i) and (ii) represent two-phase Stefan problems which either neglect or include density effects (this creates four different cases), and case (iii) assumes that the density effect is not present in the sucking problem. Case (iii) may be used as a point of reference before solving the sucking problem.

It is important to mention that PCMs have different conditions such as a subcooled growing phase in the case of solidification or a superheated consumed phase in the case of melting. With a sharp interface, the present numerical model could also reproduce these cases. However, as pointed out by Vitorino et al. [25], the low conductivity of the PCM as well as the natural convection effect in

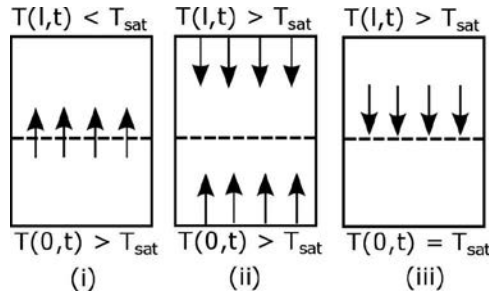


Figure 4. Boundary conditions in the cases of study. Arrows indicate the heat direction. (i) superheated phase 1 and a subcooled phase 2 (as it happens in film boiling), (ii) superheated phase 2 and a superheated phase 1 (as it happens in pool boiling), (iii) superheated phase 2 and a saturated phase 1 (as it happens in a sucking problem); (i) and (ii) consider or neglect density effects and (iii) neglect density effects (it is a simplified version of the sucking problem).

the liquid side may require to take into account the contribution of thermal resistance at the wall and also convection at the interface. In contrast, Wen et al. [26] performed simulations on heating of a flow of liquid through a channel with PCMs (a paraffin wax PCM surrounded aluminum tubes). Although the simulation neglected the thermal resistance at the wall, comparative results showed good agreement against experimental data.

3. Validation cases

This section describes the theoretical forms of Stefan problems with heat transfer in only one phase, heat transfer in two phases, and the density effects.

3.1. One-phase Stefan problems

In one-phase Stefan problems, all the heat transferred to the interface is used for phase change. The governing equation is the 1D-heat conduction equation, Eq. (10). Heat enters through a hot plate with a constant temperature as indicated by Eq. (11). The interface remains at saturated conditions and moves in proportion to the temperature gradient at the interface on the phase 1 side, as indicated by Eqs. (12) and (13), respectively. Initially, phase 1 is not present in the domain and the liquid is at a saturated temperature, as indicated by Eqs. (14) and (15).

Governing equation

$$T_t = \alpha_1 T_{yy} \quad 0 \leq y \leq Y(t) \quad (10)$$

Boundary conditions

$$T(0, t) = T_1 \quad (11)$$

Interface conditions

$$T(Y(t), t) = T_{\text{sat}} \quad (12)$$

$$\rho L Y' = -k_1 T_y(Y(t)^-, t) \quad (13)$$

Initial conditions

$$Y(0) = 0 \quad (14)$$

$$T(y, 0) = T_{\text{sat}} \quad (15)$$

In Eqs. (10)–(15), T_1 is the temperature at the bottom surface, α_1 is the thermal diffusivity of phase 1, Y' is the interface velocity, and Y is the interface position at time t . The above formulation describes

a boundary moving problem, which exact solution can be found through a similarity variable [2]. Equations (16) and (17) define the interface displacement and temperature distribution, respectively.

$$Y(t) = 2\lambda_{1st}\sqrt{\alpha_1 t} \quad (16)$$

$$T(y, t) = T_1 - (T_1 - T_{sat}) \frac{\operatorname{erf}\left(\frac{y}{2\sqrt{\alpha_1 t}}\right)}{\operatorname{erf}(\lambda_{1st})} \quad 0 \leq y \leq Y(t) \quad (17)$$

Erf stands for the error function; and λ_{1st} is a variable which is determined by the transcendental function Eq. (18).

$$\lambda_{1st} \exp(\lambda_{1st}^2) \operatorname{erf}(\lambda_{1st}) = \frac{cp_1(T_1 - T_{sat})}{L\pi^{1/2}} \quad (18)$$

3.2. Two-phase Stefan problems

The two-phase Stefan problem is a more representative case of a phase change process. In this problem, both phases are unsaturated and as a result, both phases participate in the phase change process. The governing equations and the boundary and initial conditions are described by Eqs. (19)–(26). It is important to highlight that phase 2 is now possessed by the 1D heat conduction equation, Eq. (20). Also, the mass transfer is estimated with the temperature gradients in both sides of the interface as shown by Eq. (24).

Governing equation

$$T_t = \alpha_1 T_{yy} \quad 0 \leq y \leq Y(t) \quad (19)$$

$$T_t = \alpha_2 T_{yy} \quad Y(t) < y \leq l \quad (20)$$

Boundary conditions

$$T(0, t) = T_1 \quad (21)$$

$$-k_2 T_y(l, t) = 0 \quad (22)$$

Interface conditions

$$T(Y(t), t) = T_{sat} \quad (23)$$

$$\rho LY' = -k_1 T_y(Y(t)^-, t) + k_2 T_y(Y(t)^+, t) \quad (24)$$

Initial conditions

$$Y(0) = 0 \quad (25)$$

$$T(y, 0) = T_2 \quad (26)$$

where T_2 is the temperature at the top plate and also the initial temperature of phase 2. l is the domain length (which is considered to be infinite) and α_2 is the thermal diffusivity of phase 2. The exact solution for the two-phase Stefan problem is given by Eqs. (27)–(29) [2].

$$Y(t) = 2\lambda_{2nd}\sqrt{\alpha_1 t} \quad (27)$$

$$T(y, t) = T_1 - (T_1 - T_{sat}) \frac{\operatorname{erf}\left(\frac{y}{2\sqrt{\alpha_1 t}}\right)}{\operatorname{erf}(\lambda_{2nd})} \quad 0 \leq y \leq Y(t) \quad (28)$$

$$T(y, t) = T_2 + (T_{sat} - T_2) \frac{\operatorname{erfc}\left(\frac{y}{2\sqrt{\alpha_2 t}}\right)}{\operatorname{erfc}(\nu\lambda_{2nd})} \quad Y(t) < y \leq l \quad (29)$$

Erfc stands for the complementary error function, ν is the ratio of thermal diffusivities between phases, $(\alpha_1/\alpha_2)^{1/2}$. The variable λ_{2nd} is found by the transcendental function Eq. (30).

$$\frac{cp_1(T_1 - T_{sat})}{\exp(\lambda_{2nd}^2)\text{erf}(\lambda_{2nd})} - \frac{cp_2(T_{sat} - T_2)}{\nu \exp((\nu\lambda_{2nd})^2)\text{erfc}(\nu\lambda_{2nd})} = L\lambda_{2nd}\pi^{1/2} \quad (30)$$

3.3. Stefan problems with a density effect

Due to mass conservation, $\rho_1\Delta V_1 = \rho_2\Delta V_2$, expansion of one of the phases will occur if the density in each phase is different. Such expansion introduces motion in the phase with the higher density. As a result, the heat transfer in the phase with higher density should consider a convective effect. In the case of boiling, the expansion is significant since the density ratio for the case of water is about 1,600. Welch and Wilson [6] considered the case of a planar interface with superheated liquid and saturated vapor with a large density ratio. The authors named this case as “sucking problem” since during phase change a film of liquid is sucked, causing a large expansion in the vapor. The authors compared the CFD results with a semitheoretical solution, which combines numerical and theoretical methods to determine the interface displacement and temperature distribution. The same semitheoretical procedure has been adopted by other researches [5, 24]. However, Alexiades and Solomon [2] presented a fully theoretical solution for the case of melting with different phase densities for a superheated growing phase and a subcooled consumed phase. We found that these equations are also valid for the sucking problem, which considers a high density ratio, a saturated growing phase, and a superheated consumed phase. The constitutive equations for the case of phase change with a planar interface and with density ratio are given by Eqs. (31)–(38). Phase 2, which has the higher density, is now governed by the 1D heat equation with conduction and convection, Eq. (32). The mass transfer model neglects the effect of convection, which is done to preserve the use of a similarity variable as part of the theoretical solution. Therefore, the model for mass transfer predicts interface displacements, which may be a little faster as in the real conditions.

Governing equation

$$T_t = \alpha_1 T_{yy} \quad 0 \leq y \leq Y(t) \quad (31)$$

$$T_t + \nu T_y = \alpha_2 T_{yy} \quad Y(t) < y \leq l \quad (32)$$

Boundary conditions

$$T(0, t) = T_1 \quad (33)$$

$$-k_2 T_y(l, t) = 0 \quad (34)$$

Interface conditions

$$T(Y(t), t) = T_{sat} \quad (35)$$

$$\rho LY' = -k_1 T_y(Y(t)^-, t) + k_2 T_y(Y(t)^+, t) \quad (36)$$

Initial conditions

$$Y(0) = 0 \quad (37)$$

$$T(y, 0) = T_2 \quad (38)$$

The exact solution for a planar interface model with phase change and density effect is given by Eqs. (39)–(41) [2].

$$Y(t) = 2\lambda_d \sqrt{\alpha_1 t} \quad (39)$$

$$T(y, t) = T_1 - (T_1 - T_{\text{sat}}) \frac{\text{erf}\left(\frac{y}{2\sqrt{\alpha_1 t}}\right)}{\text{erf}(\lambda_d)} \quad 0 \leq y \leq Y(t) \quad (40)$$

$$T(y, t) = T_2 + (T_{\text{sat}} - T_2) \frac{\text{erfc}\left(\frac{y}{2\sqrt{\alpha_2 t}} - \nu\lambda_d(1 - \phi)\right)}{\text{erfc}(\phi\nu\lambda_d)} \quad Y(t) < y \leq l \quad (41)$$

where ϕ is the density ratio between phases, ρ_1/ρ_2 . The variable λ_d is found by the transcendental function Eq. (42).

$$\frac{cp_1(T_1 - T_{\text{sat}})}{\exp(\lambda_d^2)\text{erf}(\lambda_d)} - \frac{cp_2(T_{\text{sat}} - T_2)}{\phi\nu \exp((\phi\nu\lambda_d)^2)\text{erfc}(\phi\nu\lambda_d)} = L\lambda_d\pi^{1/2} \quad (42)$$

Observe that $\phi = 1$ represents the case of Stefan problem with two active phases and a null density effect.

4. Results

This section presents comparative results between numerical and theoretical data. The assumed reference properties for phases 1 and 2 in the simulation are the following: $\rho_1 = 0.001 \text{ kg/m}^3$, $\rho_2 = 0.001 \text{ kg/m}^3$, $\mu_1 = 0.01 \text{ mPa s}$, $\mu_2 = 1 \text{ mPa s}$, $cp_1 = 200 \text{ J/kg-K}$, $cp_2 = 200 \text{ J/kg-K}$. Other phase change parameters include: $T_{\text{sat}} = 373 \text{ K}$ and $L = 10,000 \text{ J/kg}$. A growing superheated phase with a consumed subcooled phase assumed $k_1 = 0.005 \text{ W/m K}$, $k_2 = 0.0005 \text{ W/m K}$, $dT_1 = 10 \text{ K}$, and $dT_2 = 5 \text{ K}$. A growing superheated phase with a consumed superheated phase assumed $k_1 = 0.0005 \text{ W/m K}$, $k_2 = 0.005 \text{ W/m K}$, $dT_1 = 5 \text{ K}$, and $dT_2 = 10 \text{ K}$. These properties are used unless otherwise stated. The properties were chosen based on the previous phase change simulations in the technical literature [3, 6, 8].

The first subsection presents results for one-phase Stefan problems that either neglect or consider density effects. The results in this subsection are commonly reproduced by other studies to prove the accuracy of their mass transfer models. The findings in this subsection are a baseline for the following subsection that considers two-phase Stefan problems that either neglect or consider density effects.

4.1. One-phase Stefan problems

Figure 5 displays results for one-phase Stefan problems with a growing superheated phase and a consumed saturated phase with density ratio of one. This figure compares CFD data with theoretical data. Results report CFD data for various grids. In these results and in the results hereafter, lines represent data from the simulations and symbols represent theoretical values. The results in Figure 5 reveal that the computed results reproduce the interface displacement given by Eq. (17) accurately. Also, the results show that the grid cell length has little influence on the numerical results since the difference in the interface displacement for the various analyzed grids is hardly perceived. A grid cell size of $2,000 \mu\text{m}$ with only 20 cells in the domain gives accurate results. At 1s, the relative error of interface position is 0.01% with a $2000 \mu\text{m}$ grid. These results indicate that the adopted numerical schemes solve this case of Stefan problem with large grid cells. These results imply that the interface boundary method is an effective procedure to include the interface effects in the simulation of phase change. The interface boundary method detects the exact division between phases 1 and 2, and it also avoids the use of average properties in the interface cells. Previous simulations that solved a similar Stefan problem have used smaller grid cells. For instance, Hardt and Wondra [3] used grid cell sizes of the order of $1 \mu\text{m}$, Welch and Wilson [6] used a grid cell size of $100 \mu\text{m}$, and Sato and Niceno [5] used a grid cell size of the order of $20 \mu\text{m}$.

Figure 6 reports the interface displacement for the sucking problem (one-phase Stefan problem with density effects). The sucking problem has a growing saturated phase 1 and a consumed

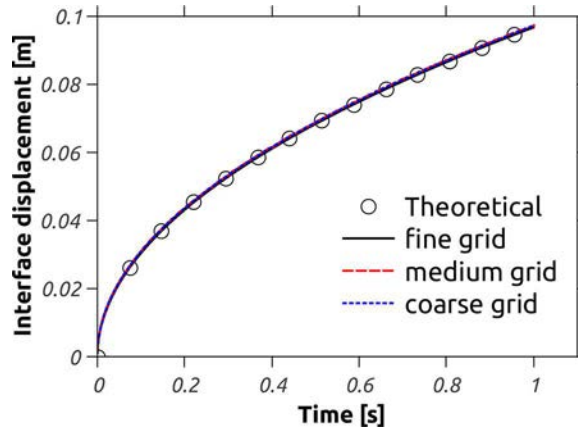


Figure 5. Interface displacement in a one-phase Stefan problem and null density effect. The grid size has a minimal effect on the results.

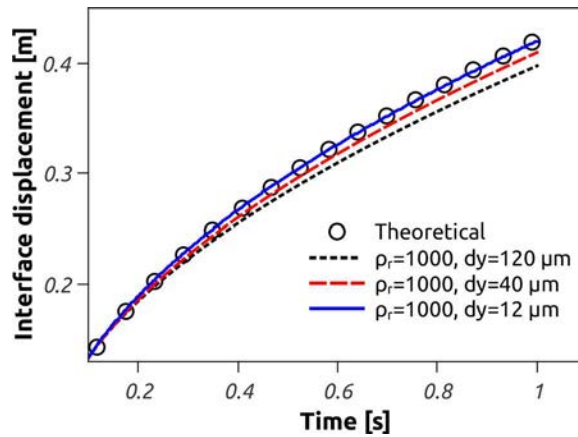


Figure 6. Interface displacement in the sucking problem. Comparison between fully theoretical and CFD results. Grid analysis on sucking problem with density ratio of 1,000. The optimal grid cell size is 12 μm .

superheated phase 2 with a density ratio of 1,000. In this problem, the vapor density was kept equal to the original value, and the liquid density was increased. The simulation was set with an increased latent heat ($L = 28,000 \text{ J/kg}$) to reduce the fast interface velocity that appears with such a high density ratio. The figure compares theoretical data given by Eq. (39) with CFD data for various grids. Equation (39) is a fully theoretical expression that is used instead of the semitheoretical procedure followed by previous works [5, 6, 24]. The simulation was initialized at 0.1s to avoid extremely thin boundary layers on the liquid side which require very refined grids to be properly resolved. The results for the sucking problem show that the grid cell size significantly influences the accuracy of the simulation. However, the accuracy increases by refining the grid. At 1s, the interface position has a relative error of 5.8, 2.9, and 0.53% with grid cell sizes of 120, 40, and 12 μm , respectively. Therefore, a grid cell size of 12 μm is needed to reproduce with good accuracy the theoretical results given by Eq. (39).

For smaller density ratios, larger grid cells can be used for a given accuracy limit. Figure 7 shows the relative error of interface displacement at 1s for density ratios of 100 and 10 with grid cell sizes of 120 and 400 μm . For a density ratio of 10, a grid cell size of 400 μm generates very accurate displacements (0.07% relative error). For a density ratio of 100, a 400 μm grid gives a relative error of 1% and a 120 μm grid reduces the relative error to 0.19%. The requirement of smaller grid cells with high

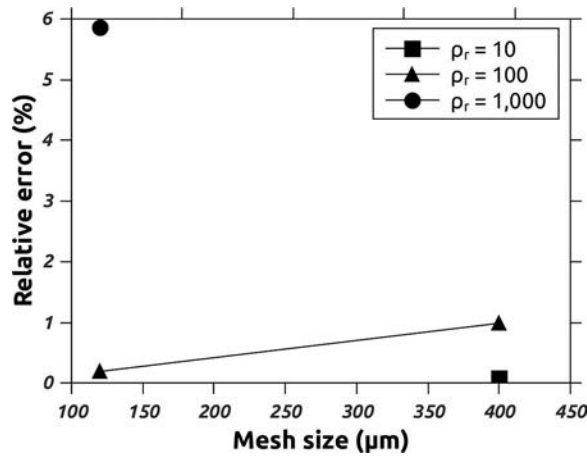


Figure 7. Relative error in interface displacement at 1s in sucking problem for various density ratios. Smaller grids are needed for good accuracy with higher density ratios.

density ratios was also observed in previous reports. Sato and Niceno [5] found a reduction in the relative error from about 5–3.3% with grid cell sizes of 50 and 12 μm . Welch and Wilson [6] found a reduction in the relative error from about 21–0.1% with grid cell sizes of 200 and 50 μm . These results show that simulations with high density ratios require more refined grids to generate accurate data. Nevertheless, the results show that data obtained with ANSYS-Fluent reproduce the sucking problem very accurately. To our knowledge, this is the first report that has solved the sucking problem in ANSYS-Fluent. This is because the technical literature lacks a method to locate the interface with the standard discretization schemes used by the software. Another important finding is that the theoretical equation, Eq. (39), represents the sucking problem very accurately. Therefore, Eq. (39) can be used as a substitute for the semitheoretical procedures followed in previous works.

To illustrate the source of the numerical errors at high density ratios, Figure 8 compares the temperature distribution at 1s in phase 2 for various density ratios. Data obtained with the theoretical Eq. (41) are reported for comparison purposes. The results show good agreement between CFD and theory for the different density ratios. The temperature distributions in Figure 8 indicate that the thermal boundary layer becomes thinner at higher density ratios. This implies that the resolution (number of cells) required to capture the thermal boundary layer in phase 2 decreases with higher density ratios. External calculations indicate that with a 120 μm grid cell size, the number of cells

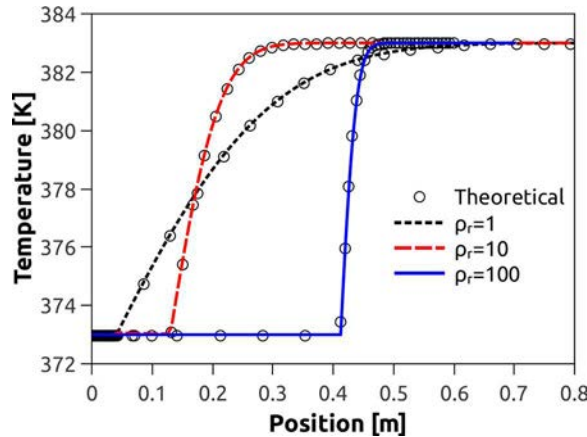


Figure 8. Temperature distributions at 1s for different density ratios. Higher density ratios develop thinner thermal films.

in the thermal boundary layer at 0.1s are 700, 222, and 73, with density ratios of 10, 100, and 1,000, respectively. The calculations consider that the cells in the thermal boundary layer are the cells with a temperature below 382.99 K. Therefore, the source of the numerical errors is the physical formation of a thin thermal boundary layer at high-density ratios, which requires small cells to be properly captured.

4.2. Two-phase Stefan problems

To the knowledge of the present authors, this is the first report that compares numerical simulations of liquid–vapor phase change with heat transfer in both phases against theoretical data. Previous works simulated fundamental problems with heat transfer in just one phase. Other works have simulated phase change with heat transfer in both phases, but their mass transfer model was compared against Stefan problems with a saturated phase [5, 24]. A comparison between CFD and theory with heat transfer in the two phases and with density effects is a more sophisticated alternative to prove the accuracy of phase change simulations with heat transfer in both phases. The present simulation considers a density ratio of 10. This avoids the formation of thin thermal films that require refined grids, which lead to large computational times. The grid cell size chosen to perform the simulation was 400 μm —an average grid cell size for the adopted numerical schemes.

Figure 9 displays the results for two-phase Stefan problems with a growing superheated phase and a consumed subcooled phase [case (i) in Figure 4]. Results for one-phase Stefan problem with a superheated growing phase and a saturated consumed phase are also reported for comparison purposes. The case with a higher density considers also a higher thermal conductivity in phase 2 (0.005 W/m K). In these two-phase Stefan problems, phase 1 is transferring heat to the interface; part of this heat goes to phase 2 as sensible heat, and the rest is used for evaporation. The simulation considers subcooled levels of 0 and 5 K, with density ratios of 1 and 10. The results in the figure show that the results from the simulation and the theoretical data have good agreement. At 1s, the interface position has a relative error of less than 0.5 % for each analyzed case. As it is shown in the figure, higher subcooling levels and density ratios reduce the interface velocity. For instance, the interface positions at 1s with $dT_2 = 0$ K and $\rho_r = 1$, with $dT_2 = 5$ K and $\rho_r = 1$, and with $dT_2 = 5$ K and $\rho_r = 10$, are 0.097, 0.091, and 0.072 m, respectively. The velocity of the interface is reduced because part of the heat arriving to the interface is lost as sensible heat into the subcooled phase, which decreases the amount of energy for phase change. Also, the case with a higher density ratio has a larger phase 2 thermal conductivity, which contributes to an increase in the sensible heat transfer into phase 2 and a decrease in the

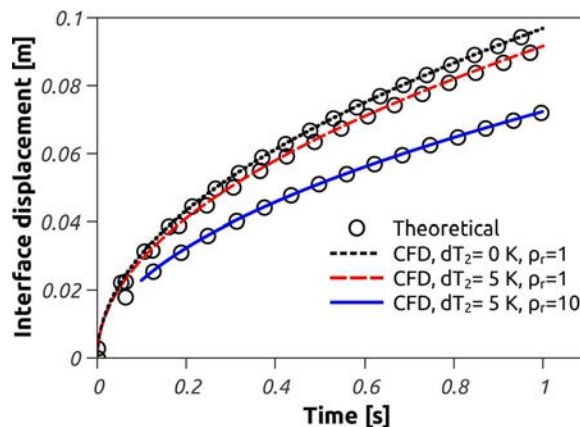


Figure 9. Interface displacement in two-phase Stefan problems with a growing superheated phase, and a consumed subcooled phase. The temperature gradient in phase 2 reduces the phase change rate. A higher density reduces the mass transfer due to large temperature gradients in phase 2.

amount of energy available for phase change. Although these results may not represent the actual physical conditions in film boiling, they indicate that the adopted numerical schemes accurately simulate phase change with two active phases. This implies that the numerical procedures can be used to simulate the actual process. The purpose of this work is not to uncover the effect of physical properties, but to describe benchmark problems for the simulation of phase change with heat transfer in two phases, and how these problems could be solved in ANSYS-Fluent.

Figure 10 shows interface displacements for two-phases Stefan problems with a consumed superheated phase and a growing superheated phase [case (ii) in Figure 4]. Results for a one-phase Stefan problem with a saturated growing phase and a consumed superheated phase without density effect are also reported [case (iii) in Figure 4]. In two-phase Stefan problems, both phases are transferring heat to the interface. This implies that both sides of the interface contribute to the mass transfer. The figure compares the results of the simulations with the theoretical data. The results show data for superheat levels in the growing phase (phase 1) of 0 and 5 K. The superheat level in the consumed phase (phase 2) is 10 K. Also, the 5 K superheat level considers density ratios of 1 and 10. The CFD results agree well with the theory. At 1 s, the interface position has a relative error of less than 0.3% for each case. The results also show that the interface velocity with a 5 K superheated level is faster than the 0 K superheated level with the same density ratio. The results with different density ratio show that the interface displacement is faster if the phase 2 density increases. The faster interface displacement with two active phases at the same density ratio (relative to one active phase) can be explained by the fact that both phases are transferring heat to the interface, and therefore, the amount of energy used for phase change is higher. The interface is much faster with a density ratio of 10 because a thinner thermal film with a large temperature gradient appears at higher densities. This is because the faster evaporation rate prevents the spreading of the thermal layer. The large temperature gradient increases the mass transfer.

Figure 11(a) shows the temperature distribution in a growing superheated phase and in a consumed subcooled phase [case (i) in Figure 4], while Figure 11(b) shows the results of a growing superheated phase and a consumed superheated phase [case (ii) in Figure 4]. Results for one-phase Stefan problems without density effects are also reported for comparison purposes. The results in Figure 11(a) with a higher density consider a higher thermal conductivity in phase 2 (0.005 W/m K). The importance of these results lies in the fact that previous numerical works have shown temperature distributions in only one phase, whereas the other phase was always saturated. The temperature distributions in both phases show very good agreement between the theoretical equations and CFD. A

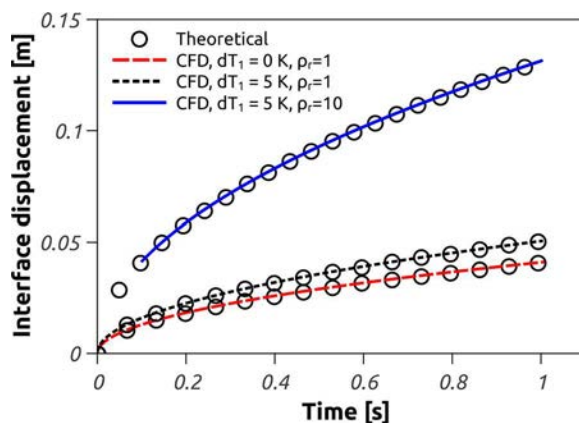


Figure 10. Interface displacement in two-phase Stefan problems with a growing superheated phase and a consumed superheated phase. Comparison between theory and CFD. Transfer of heat to the interface with both phases increases the interface velocity. A higher density increases the mass transfer due to large temperature gradients in phase 2.

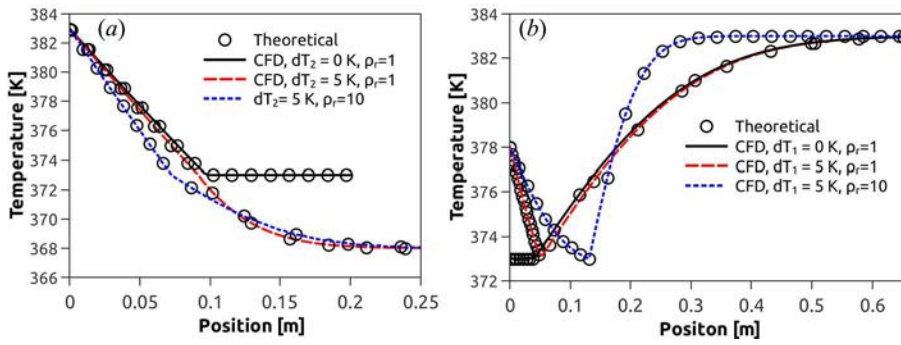


Figure 11. Temperature distribution in two-phase Stefan problem. Comparison between theory and CFD. (a) Superheated growing phase and subcooled consumed phase (b) Superheated growing phase and superheated consumed phase. A higher density increases the temperature gradients in phase 2.

comparison of the temperature profiles between phase 1 and phase 2 in Figure 11(a) shows that phase 1 has a higher temperature gradient relative to phase 2 with a density ratio of 1. The increase in density of phase 2 should lead to a thinner thermal layer, but the case with a higher density ratio has a larger conductivity. The larger conductivity decreases the temperature gradient by enhancing the heat transfer.

The results with two superheated phases in Figure 11(b) show that for the analyzed conditions, both phases have similar temperature gradients if they have the same density. However, a phase 2 with a higher density leads to a higher temperature gradient at the interface, and as a result, the mass transfer increases. Furthermore, the results in Figure 11(b) indicate that the temperature gradient in phase 1 is smaller if the density of phase 2 increases. This is because the interface has a velocity such that phase 1 is unable to transfer the required heat to maintain a significant temperature gradient at the interface. In other words, phase 2 with a higher density increases the interface velocity, which reduces the effect of phase 1 in the mass transfer process. These results explain the behavior in previous simulations of pool boiling, which show that the superheated vapor has a null effect on the growing rate of a bubble [5, 24]. The effect may be minimal because the liquid properties generate an interface velocity such that the vapor (with a low thermal conductivity) is unable to transfer the required heat to maintain a significant temperature gradient at the interface.

5. Conclusion

In this work, a numerical approach is presented to simulate phase change with heat transfer in both phases and density effects for a planar interface. The numerical schemes used the interface location in the discretization of the fluxes in the cells next to the interface cells. The simulation calculated the mass transfer with temperature gradients at the interface. Volume-of-Fluid (VOF) tracked the interface location. The simulation was done in ANSYS-Fluent with User-Defined Functions (UDFs) that accounted for the heat and mass transfer at the interface. The numerical results were compared against fully theoretical equations with good agreement.

Simulations of phase change should locate the interface to estimate an accurate mass and energy transfer between phases. The present work introduced an interface boundary method in which the faces of the neighboring cells were extended to the interface location. The diffusive and convective terms in the neighboring cells consider the interface location as part of their discretization. The neighboring cells ignore the interface cell. This eliminates errors that appear with the use of average properties in the interface cell. The interface boundary method lacks interpolation or extrapolation functions. The mass transfer model determines the temperature gradients at the interface cell with the VOF value and with the temperature of the neighboring cells. The location of the interface

and the estimation of the mass transfer with the VOF value at the interface cell were easy to implement and gave accurate interface displacements and temperature distributions.

ANSYS-Fluent is an attractive software for simulation, since it solves the governing equations for mass, momentum, and energy conservation. The software needs to be customized to simulate phase change with a sharp interface. At present, the technical literature lacked of a simulation within ANSYS-Fluent that solved Stefan problems with density effects. The present work used ANSYS-Fluent to solve these fundamental problems. However, the software was extensively modified. UDFs initialized the simulation, adjusted the numerical methods at the interface, located the interface, customized the thermal properties at the cells next to the interface, estimated the mass transfer at each time step, and defined mass source terms in the VOF equation. The results indicated that the software performs accurate phase change simulations if it is properly customized.

Previous numerical studies solved Stefan problems with heat transfer in only one phase. However, there are important cases in which the phase change process is affected by the heat transfer in both phases. The present work used Stefan problems with heat transfer in both phases and with density effects. All the simulations matched in good agreement with the interface displacement and temperature distributions of the theoretical data. The present work proved that there is no need to use semitheoretical models to represent fundamental problems for phase change with density effect. Moreover, the results indicated that CFD performed an accurate mass transfer with heat transfer in both phases. To our knowledge, this is the first report that compared a numerical model for phase change against theoretical solutions with two active phases. This implies that the present work has extended the alternatives to perform and analyze numerical models on phase change.

Funding

The work was performed in the Thermal Analysis, Microfluidics, and Fuel Cell Laboratory in the Mechanical Engineering Department at the Rochester Institute of Technology, NY. The authors gratefully acknowledge the financial support provided by the National Science Foundation under Award No. 1511314.

References

- [1] J. Crepeau, Josef Stefan: His Life and Legacy in the Thermal Sciences, *Exp. Therm. Fluid Sci.*, vol. 31, pp. 795–803, 2007.
- [2] V. Alexiades and D. Solomon, *Mathematical Modeling of Melting and Freezing Processes*, chap. 2, Hemisphere, Washington, DC/New York, 1993.
- [3] S. Hardt and F. Wondra, Evaporation Model for Interfacial Flows based on a Continuum-field Representation of the Source Terms, *J. Comput. Phys.*, vol. 227, pp. 5871–5895, 2008.
- [4] H. Thakur, K. M. Singh, and P. K. Sahoo, Phase Change Problems Using the MLPG Method, *Numer. Heat Transfer A, Appl.*, vol. 59, pp. 438–458, 2011.
- [5] Y. Sato and B. Niceno, A Sharp-interface Phase Change Model for Mass-conservative Interface Tracking Method, *J. Comput. Phys.*, vol. 249, pp. 127–161, 2013.
- [6] S. W. J. Welch and J. Wilson, A Volume of Fluid Based Method for Fluid Flows with Phase Change, *J. Comput. Phys.*, vol. 160, pp. 662–682, 2000.
- [7] G. Son and V. K. Dhir, Numerical Simulation of Film Boiling Near Critical Pressures with a Level-set Method, *J. Heat Transfer*, vol. 120, pp. 183–192, 1998.
- [8] D. L. Sun, J. L. Xu, and L. Wang, Development of a Vapor-liquid Phase Change Model for Volume-of-fluid in Fluent, *Int. Commun. Heat Mass Transfer*, vol. 39, pp. 1101–1106, 2012.
- [9] D. Z. Guo, D. L. Sun, Z. Y. Li, and W. Q. Tao, Phase Change Heat Transfer Simulation for Boiling Bubbles Arising from a Vapor Film by the VOSET Method, *Numer. Heat Transfer A Appl.*, vol. 59, pp. 857–881, 2011.
- [10] D. Sun, J. Xu, and Q. Chen, Modeling of the Evaporation and Condensation Phase-change Problems with Fluent, *Numer. Heat Transfer B, Fund.*, vol. 66, pp. 326–342, 2014.
- [11] D. Banerjee and V. K. Dhir, Study of Film Boiling on a Horizontal Disc: Part I-analysis, *J. Heat Transfer*, vol. 123, p. 271, 2001.
- [12] J. Gyls, R. Skvorcinskiene, L. Paukstaitis, M. Gyls, and A. Adomavicius, Film Boiling Influence on the Spherical Body's Cooling in Sub-cooled Water, *Int. J. Heat Mass Transfer*, vol. 95, pp. 709–719, 2016.

- [13] M. Augspurger and H. S. Udaykumar, A Cartesian Grid Solver for Simulation of a Phase-change Material (PCM) Solar Thermal Storage Device, *Numer. Heat Transfer B Fund.*, vol. 69, pp. 179–196, 2016.
- [14] M. D. Muhammad, O. Badr, and H. Yeung, Validation of a CFD Melting and Solidification Model for Phase Change in Vertical Cylinders, *Numer. Heat Transfer A Appl.*, vol. 68, pp. 501–511, 2015.
- [15] J. Zhang, G. A. Sandison, J. Y. Murthy, and L. X. Xu, Numerical Simulation for Heat Transfer in Prostate Cancer Cryosurgery, *J. Biomech. Eng.*, vol. 127, pp. 279–294, 2005.
- [16] A. Fortin and Y. Belhamadia, Numerical Prediction of Freezing Fronts in Cryosurgery: Comparison with Experimental Results, *Comp. Meth. Biomech. Biomed. Eng.*, vol. 8, pp. 241–249, 2005.
- [17] C. W. Hirt and B. D. Nichols, Volume of Fluid (VOF) Method for the Dynamics of Free Boundaries, *J. Comput. Phys.*, vol. 39, pp. 201–225, 1981.
- [18] R. Fedkiw, T. Aslam, B. Merriman, and S. Osher, A Non-oscillatory Eulerian Approach to Interfaces in Multimaterial Flows (the Ghost Fluid Method), *J. Comput. Phys.*, vol. 152, pp. 457–492, 1999.
- [19] F. Gibou, L. Chen, D. Nguyen, and S. Banerjee, A Level Set Based Sharp Interface Method for the Multiphase Incompressible Navier–Stokes Equations with Phase Change, *J. Comput. Phys.*, vol. 222, pp. 536–555, 2007.
- [20] S. Tanguy, M. Sagan, B. Lalanne, F. Couderc, and C. Colin, Benchmarks and Numerical Methods for the Simulation of Boiling Flows, *J. Comput. Phys.*, vol. 246, pp. 1–22, 2014.
- [21] Y. Zhang, K. Du, J. P. He, L. Yang, and Y. J. Li, Impact Factors Analysis of the Enthalpy Method and the Effective Heat Capacity Method on the Transient Non-linear Heat Transfer in Phase Change Materials (PCMs), *Numer. Heat Transfer A Appl.*, vol. 65, pp. 66–83, 2014.
- [22] P. A. Galione, O. Lehmkuhl, J. Rigola, and A. Oliva, Fixed-grid Modeling of Solid–Liquid Phase Change in Unstructured Meshes Using Explicit Time Schemes, *Numer. Heat Transfer B Fund.*, vol. 65, pp. 27–52, 2014.
- [23] M. W. Akthar and S. J. Kleis, Boiling Simulations on Adaptive Octree Grids, *Int. J. Multiphase Flow*, vol. 53, pp. 88–99, 2013.
- [24] C. Kunkelmann and P. Stephan, CFD Simulation of Boiling Flows Using the Volume-of-fluid Method within OpenFOAM, *Numer. Heat Transfer A Appl.*, vol. 56, pp. 631–646, 2009.
- [25] N. Vitorino, J. C. C. Abrantes, and J. R. Frade, Solutions for Heat or Cold Discharge from Encapsulated Phase-change Materials, *Numer. Heat Transfer B Fund.*, vol. 64, pp. 421–435, 2014.
- [26] S. Wen, E. Fleming, L. Shi, and A. K. da Silva, Numerical Optimization and Power Output Control of a Hot Thermal Battery with Phase Change Material, *Numer. Heat Transfer A Appl.*, vol. 65, pp. 825–843, 2014.